EURASIP Journal on Wireless Communications and Networking

RESEARCH Open Access

Application research of polar coded OFDM underwater acoustic communications

Yushuang Zhai[1,2], Jilong Li[1*], Haihong Feng[1] and Feng Hong[1]

*Correspondence:
lijilong@mail.ioa.ac.cn

[1] Shanghai Acoustics Laboratory, Chinese Academy of Sciences, Shanghai 201815, China
[2] University of Chinese Academy of Sciences, Beijing 100049, China

Abstract

To further accelerate the practical process of polar codes in underwater acoustic communication (UWC) and improve the reliability and efficiency of underwater data transmission, we first propose a polar code construction method suitable for the underwater acoustic channel, which drastically reduces the complexity and meets the need for practical UWC. Then, we establish a practical polar coded UWC scheme by devising a two-step procedure based on the Orthogonal Frequency Division Multiplexing technique. Moreover, through simulation, the scheme's performances with the unimproved and the proposed polar code construction method are analyzed. Moreover, its performances with four different polar decoders are also given. The performance comparison with the LDPC coded UWC system is studied as well. Furthermore, lake-trial results under two different channel conditions demonstrate that the proposed construction method and the scheme effectively guarantee the reliability of data transmission, achieving error-free transmission at a transmission distance of 1718 m with the signal-to-noise-ratio (SNR) of 21 dB, and a transmission distance of 749 m with the SNR of 16.5 dB, better than the LDPC coded system with same conditions. The semi-experimental results show that the proposed polar coded system under the Cyclic Redundancy Check-Aided Successive Cancellation List decoder outperforms the LDPC coded system by approximately 2.1–3.7 dB.

Keywords: Channel coding, OFDM, Polar code, Underwater acoustic communication

1 Introduction

Underwater acoustic communication (UWC) is widely used for environmental monitoring, exploration of the oceans, military missions, controlling underwater equipment over large areas in quasi-real-time, assisting localization, and navigation [1, 2]. However, the UWC through the underwater acoustic (UWA) channel, especially the shallow water channel, proves challenging due to parameters that randomly vary in spatial/temporal/frequency aspects, large attenuation, severe multipath effects, strict band-limited property, high noise level, and low sound velocity [3, 4]. In recent years, the digital UWC has raised vast concerns about the use of bandwidth-efficient modulation and channel coding techniques [5, 6]. Of these, the Orthogonal Frequency Division Multiplexing (OFDM) has been extensively used in short-range, high-rate UWC systems since its capability of inter-symbol interference (ISI) removal, low receiver complexity,

and robustness against large delay spread [7, 8]. To combat the significant interference among OFDM subcarriers caused by the high temporal and spatial variability of channel conditions, channel coding approaches are applied [7, 9], which drastically improve the system performance by introducing both diversity gain and coding gain through redundant signaling. Over the past two decades, Turbo code and Low-density Parity-Check (LDPC) code have been widely studied and applied in UWC [7, 10–12], both of which have brought capacity-approaching performance within reach of implementable systems. However, the high complexity of the above two codes, under practical constraints such as limited decoding delay and high spectral efficiency, is still a major hurdle for low power and real-time implementations in practical UWC [13]. There is a need for new methods that simplify code design, construction, storage, and decoder implementation. Polar code, a new class of provably capacity-achieving code invented by Arikan [14], has become the subject of active research in nowadays channel coding area due to its explicit construction, low-complexity encoding, and decoding algorithms [15]. It has been extended to numerous communications settings [16] with significant improvements in channel-specific code construction [14, 17–22], and decoding literature [23–26]. It has been proved to be a fierce competitor of turbo and LDPC codes. However, in UWA channels, the theoretic proofs and performance of polar codes are relatively far less analyzed. The prior channel-dependent constructions [20, 21] cannot reveal the explicit relationship between the fading channel parameters and the error probability of the polarized channel. Due to the unique characteristics of UWA channels, most existing construction methods cannot be tailored to the specific UWC.

Recently, the research on polar codes in UWC has involved the fields of multi-user communication [27], high-order modulation [28], cascading code [29], and joint source/channel coding [30]. For the construction of polar codes in the UWA channel, Bhattacharyya bounds [27, 31–33] and Monte Carlo (MC) [31, 34] approaches are commonly used. However, the bounds of the former are not guaranteed to be strict, and the latter requires a large number of iterations of the Monte-Carlo simulation. Lidström [35] used Tal and Vardy's construction algorithm, which is based on an upper bound on discrete binary-symmetric channels. However, this algorithm requires high number of quantization levels in order to achieve reasonable precision. In [36], the Gaussian approximation (GA) method is used to construct the polar code. However, the implementation is relatively complex since it needs to be assisted by the decision feedback equalization (DFE) and the hybrid automatic repeat request (HARQ) mechanism. Additionally, OFDM is not taken into account in this method. Thus, one of aims of this paper is to propose a practical polar code construction method for OFDM UWC. With details of the implementation, we present a novel polar code construction method combining MC simulation-based method and GA method. Considering the uncertainty of UWA channels cannot be characterized and fading statistics are not available, we use the MC simulation-based method to find the information set. Moreover, to further reduce the computational complexity of estimation of polarized subchannel error probability, we optimize the GA method for the proposed parallel OFDM channel, with a simpler channel estimation.

Moreover, to the extent of the author's knowledge, no application of polar coded OFDM to the UWC has been published at the time of writing, other than for simulations [27, 31,

34] or tank tests [27], nor its use together with the polar code construction method defined here. Thus, in this paper, we also present the detailed performance results of the proposed system through simulation and lake tests, including the performance of polar code construction methods before and after improvement, the robustness to slow time-varying channels, and the performance under four different decoding methods.

Main contributions of this paper can be summarized to the following three aspects. Firstly, we design a novel polar code construction method for the UWA channel, based on the MC simulation algorithm [14] and the GA method [19] with details of the specific implementation. Secondly, we establish a practical and reliable polar coded UWC scheme by devising a two-step procedure. Thirdly, we verify and evaluate the performance of the proposed polar construction method and the polar coded OFDM UWC scheme, with detailed analysis and lake trial experimental verification.

This paper starts with the background of the polar code in Section II. Next, in Sections III, we introduce the UWA channel model and propose the novel polar code construction method. To verify the proposed polar code construction method and analyze the application performance of polar code in the UWC OFDM system, in Section IV, we establish a practical and reliable polar coded UWC scheme. Then simulations are performed in Section V. Finally, in Section VI, lake trial experiments are conducted at two sites in the Qiandao Lake to verify the practical applicability of the proposed polar coded UWC scheme. Finally, the conclusion is given in Section VII.

2 Polar code

2.1 Channel polarization and polar code construction

The construction of polar codes relies on the phenomenon of *channel polarization* [14]. For a given binary input discrete memoryless channel (BDMC) $W : \mathcal{X} \to \mathcal{Y}$ with input alphabet $\mathcal{X} = \{0, 1\}$ and output alphabet $\mathcal{Y}$, the channel transition probabilities can be defined as $W(y|x), x \in \mathcal{X}$ and $y \in \mathcal{Y}$. The operation of channel polarization consists of a channel combining phase and a channel splitting phase, by which one manufactures out of $N = 2^n, n = 1, 2, \cdots$ independent copies of the given BDMC W the second set of N polarized subchannels $W_N^{(i)} : \mathcal{X} \to \mathcal{Y} \times \mathcal{X}^{i-1}, i \in [1, N]$ with the transition probabilities

$$W_N^{(i)}\left(y_1^N, u_1^{i-1}|u_i\right) = \sum_{u_{i+1}^N \in \mathcal{X}^{N-i}} \frac{1}{2^{N-1}} W_N\left(y_1^N|u_1^N\right), \tag{1}$$

where

$$W_N\left(y_1^N|u_1^N\right) = \prod_{i=1}^{N} W\left(y_i|x_i\right), \tag{2}$$

and $x_1^N = u_1^N \mathbf{G}_N$. $\mathbf{G}_N = \mathbf{B}_N \mathbf{F}_2^{\otimes n}$ is the generator matric, in which $\mathbf{B}_N$ is the bit-reversal permutation matrix and $\mathbf{F}_2^{\otimes n}$ is n-fold Kronecker product of Arikan's standard polarizing kernel, where

$$\mathbf{F}_2 = \begin{bmatrix} 1 & 0 \\ 1 & 1 \end{bmatrix}. \tag{3}$$

As $N \to \infty$, channel polarization results in $NI(W)$ noiseless channels having near-1 capacity and $N(1 - I(W))$ purely noisy channels having near-0 capacity. Virtually error-free transmission can be achieved by sending the data over noiseless subchannels. [14]. For the finite code length, before encoding, it becomes necessary to calculate the reliability of all the bit-subchannels and select the most reliable bit-subchannels to carry the information bits. This selection of bit-subchannels completely defines a polar code and therefore is called the *polar code construction* [14]. Since the reliability calculation of all the bit-subchannels relies on characteristics and transmission parameters of underlying component channels, most of the existing polar code construction algorithms [14, 17–22] are channel specific and are hence not universal, which includes for example the Bhattacharyya parameter method for binary erasure channel (BEC) [14], Density Evolution (DE) method [17] and Tal & Vardy's upgrading and degrading method [18] for arbitrary symmetric BDMCs, the GA method [19] for additive white gaussian noise (AWGN) channels, and several heuristic constructions for fading channel e.g. [20, 21]. Additionally, MC simulation method proposed in [14], can be applied to a wide range of channels, such as UWA channels, however, its computational complexity is the largest among all existing methods. For composing the proposed polar coded UWC system scheme in this paper, we present a novel polar code construction method related to UWA channel characteristics and introduce its implementation in Section III.

2.2 Polar encoding

Take the binary sequence u_1^N with the finite code length N as an example. Before encoding, construct polar codes $(N, K, \mathcal{A}^c)$ by selecting K good noiseless subchannels $\mathcal{A}$ to transmit information bits $u_{\mathcal{A}}$, while distributing frozen bits $u_{\mathcal{A}^c}$, taken here as zeros, to the $N - K$ unreliable noise ones $\mathcal{A}^c$. After polar code construction, the polar codeword can be generated by $x_1^N = u_1^N \mathbf{G}_N$. The illustration of the polar encoder with parameter $(N, K, \mathcal{A}^c) = (8, 4, \{0, 1, 2, 4\})$ is depicted in Fig. 1a.

2.3 Polar decoding

In Arıkan's seminal paper [14], a direct implementation of the successive-cancellation (SC) decoder is given based on the recursive calculations of the path metrics and the factor graph representation of polar codes. The SC decoder [14] essentially follows the same encoder diagram in Fig. 1b using decoding operations that resemble one iteration of the classic belief propagation (BP) algorithm. Let $L_\lambda(\phi, \beta)$ be the log-likelihood (LLR) value and $B_\lambda(\phi, \beta)$ be the bit decisions, computed from already detected known bits, of the node ϕ in the node group β at a depth λ in the graph. The SC decoder computes the estimated message vector $\hat{u}_i$ by

$$\hat{u}_i = \begin{cases} 0 & \text{if } i \in \mathcal{A}^c \text{ or } L_n(i, 0) \geq 0 \\ 1 & \text{otherwise} \end{cases}. \tag{4}$$

$L_\lambda(\phi, \beta)$ evolve in the reverse direction from right to left and $B_\lambda(\phi, \beta)$ are made at the left end of the circuit and broadcasted to the rest of the circuit. By going from $i = 0$ to $N - 1$ in increasing order, where $L_n(i, 0)$ is computed using the recursion

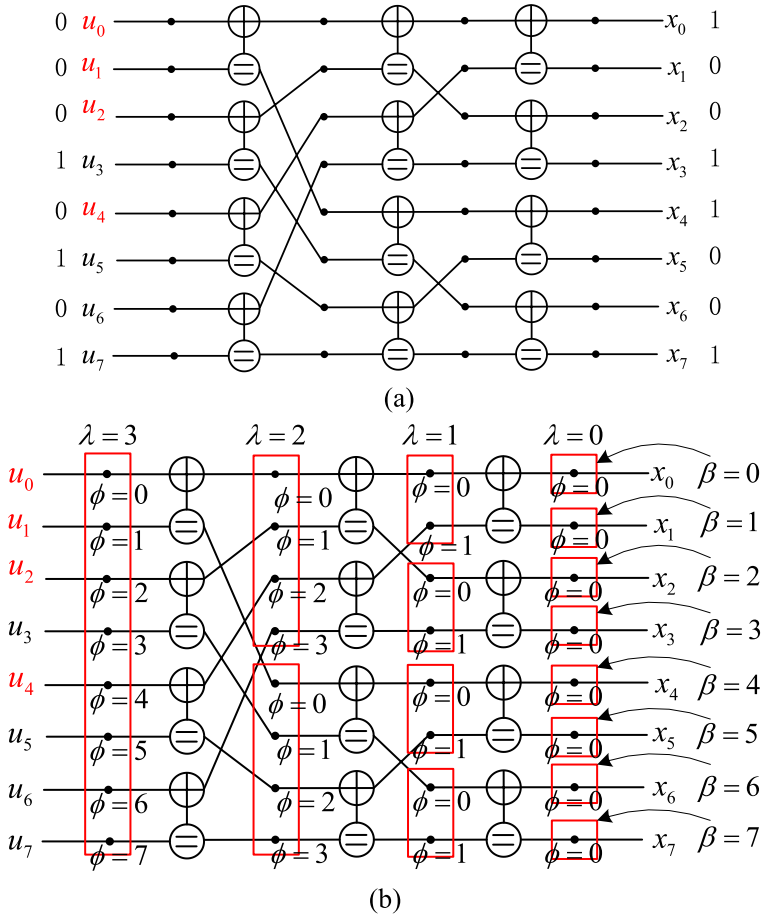

Fig. 1 **a** Illustration of Arikan's $\mathcal{O}(N \log N)$ complexity encoder implementation with $(N, K, \mathcal{A}^c) = (8, 4, \{0, 1, 2, 4\})$ (**b**) SC decoder factor graph and notation

$$L_\lambda(\phi, \beta) = \begin{cases} L_{\lambda-1}(\psi, 2\beta) \boxplus L_{\lambda-1}(\psi, 2\beta+1), \ \phi \ is \ odd \\ L_{\lambda-1}(\psi, 2\beta+1) + (-1)^{B_\lambda(\phi-1,\beta)} L_{\lambda-1}(\psi, 2\beta), \ \phi \ is \ even \end{cases}, \tag{5}$$

where $\boxplus$ is defined as

$$a \boxplus b = 2 \tanh^{-1}\left(tanh\left(\frac{a}{2}\right) tanh\left(\frac{b}{2}\right)\right). \tag{6}$$

And update the B matrix by

$$B_{\lambda-1}(\psi, 2\beta) = B_\lambda(\phi, \beta) \oplus B_\lambda(\phi - 1, \beta), \tag{7}$$

$$B_{\lambda-1}(\psi, 2\beta + 1) = B_\lambda(\phi, \beta), \tag{8}$$

where $\oplus$ is binary XOR operation and $\psi = \lfloor \phi/2 \rfloor$.

Besides the SC decoder, there are also other decoding methods as follows. In the SC-List (SCL) decoder, instead of decoding a single codeword, a list of L tentative codewords is decoded simultaneously, and the final codeword can be selected with

the help of a cyclic redundancy check (CRC) [23]. The BP decoder of polar codes is first introduced by Arikan in [24], based on the factor graph representation, which is equivalent to the trellis of polar code shown. Rather than exchanging the hard messages, soft messages are iteratively propagated in the graph until the maximum number of iterations is reached. Then the estimated codewords are generated by applying threshold detection on the left-hand-side messages. The soft cancellation (SCAN) decoder [25], a soft-input soft-output version of the SC decoder, calculates extrinsic LLRs of both the uncoded and encoded bits using the recursive formulas and passes perfect information about frozen bits by assigning a higher LLR value on the nodes corresponding to $\mathcal{A}^c$. It provides the soft outputs with low complexity that many practical applications require concatenated coding or turbo equalization scheme.

3 A novel polar code construction method for the UWA channel

3.1 UWA channel model

To propose a polar code construction method for the UWA channel and measure the reliability of polarized bit-subchannels effectively, this section starts by developing a UWA channel model. Then we analyze the polarized bit-subchannels under the OFDM UWA channel model.

In this paper, the UWC scenario is considered as a single-input-single-output (SISO) information transmission in the horizontal direction between two fixed points in the shallow sea. In this scenario, it is assumed that the depth of the channel, the transmission distance, and the positions of the transmitting and receiving transducers change little during the communication process. Considering the reflection and refraction of the inhomogeneous medium in seawater, the sea surface, and the seabed, the acoustic wave propagation in the shallow sea channel has a time-varying multipath structure. The multipath delay is between tens and hundreds of milliseconds, and the signal exhibits frequency-selective fading characteristics. Based on the above analysis, we model the UWA channel referring to [37] by taking into account physical and statistical properties.

(1) For the statistical part, the channel is assumed wide sense stationary and uncorrelated scattering (WSSUS) and modeled by a sum of several multipath components. The continuous-time statistical channel impulse response (CIR) $b(\tau, t)$ and its corresponding transfer function $B(f, t)$ can be given as

$$b(\tau,t)=\sum_{p=0}^{P-1} b_p(t)\delta\left(\tau-\tau_p\right), B(f,t)=\sum_{p=0}^{P-1} b_p(t)e^{-j2\pi f\tau_p}, \tag{9}$$

where P is the number of arrival paths, $b_p(t)=b_p e^{j2\pi D_p t}$, where b_p, τ_p and D_p denote the cumulative reflection coefficient, the time delay, and the Doppler shift along the p-th propagation path, respectively.

(2) For the physical part, the path loss is a combination of the geometric spreading and absorption, which can be written as a function of both the distance and signal frequency

$$Q^2(d,f) = d^{-sp}\left(q^2(f)\right)^{-d}, \tag{10}$$

where d is the transmission distance (m) and f is the frequency in kHz. d^{-sp} represents the spreading loss and sp is the spreading factor. $q^2(f)$ is the absorption coefficient given by [38, Eq. (3.4.29)]. Let $\chi_{d_p}(\tau)$ denote the p-th path loss CIR corresponding to $Q(d_p,f)$,i.e.,$Q(d_p,f) = \int \chi_{d_p}(\tau)\exp(-j2\pi f\tau)d\tau$.

Taking into account the above two properties, the UWA cannel CIR $h(\tau,t)$ can be written as

$$h(\tau,t) = \chi_d(\tau) \otimes b(\tau,t) = \chi_d(\tau) \otimes \sum_{p=0}^{P-1} b_p(t)\delta(\tau-\tau_p), \tag{11}$$

and the channel transfer function $H(f,t)$ can be written as

$$\begin{aligned} H(f,t) &= \int h(\tau,t)e^{-j2\pi f\tau}d\tau = \sum_{p=0}^{P-1} b_p(t)Q(d_p,f)e^{-j2\pi f\tau_p} \\ &\approx Q(d_0,f)\sum_{p=0}^{P-1} b_p(t)e^{-j2\pi f\tau_p} = Q(d,f)B(f,t). \end{aligned} \tag{12}$$

Since the relative motion of the transmitter and receiver is not considered, it is assumed that the channel is quasi-stationary during several OFDM blocks and that it is slowly changing over different periods. The coherence time is assumed to be large enough to support polar code construction a few seconds ahead, while channel stability is ensured over a long enough interval of time by appropriate Doppler compensation.

Next, the polarized bit-subchannels of the OFDM UWC system are analyzed based on the above UWA channel model. For a polar code of code length N in the OFDM UWC system, the channel polarization described in [14] is extended to the case of communications over N parallel flat fading channels $W_1 : \mathcal{X} \to \mathcal{Y}, W_2 : \mathcal{X} \to \mathcal{Y}, \ldots W_N : \mathcal{X} \to \mathcal{Y}$, located at data subcarriers S_D, as shown in Fig. 2.

The underlying channels $W : \{W_a|H_a : \mathcal{X} \to \mathcal{Y}\}, a \in S_D$ of the channel polarization transformation are no longer used of the same channel. On each data subcarrier, the channel transition probability density function can be written as:

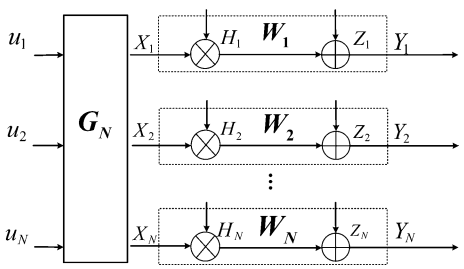

Fig. 2 Polar coding in OFDM parallel channels

$$W(Y_a, H_a|X_a) = \int_0^{\infty} p(H_a) \frac{1}{\sqrt{2\pi\sigma_a^2}} e^{-\frac{(Y_a - H_a X_a)^2}{2\sigma_a^2}} \mathrm{d}H. \tag{13}$$

where $p(H_a)$ is the distribution probability density function of H_a.H_a and σ_a^2 is the channel gain and the noise variance at the a-th subcarrier, respectively. In the practical UWC process, we can assume that the instantaneous channel side information (CSI) is known at the receiver by channel estimation. Substituting fading coefficients H_a, noise variance σ_a^2 into Eq. (13), the $W(Y_a, H_a|X_a)$ can be simplified as

$$W(Y_a, H_a|X_a) = \frac{1}{\sqrt{2\pi}\sigma_{na}} e^{-\frac{|Y_a - H_a X_a|^2}{2\sigma_{na}^2}}. \tag{14}$$

During the polarization transformation, the conditional transition probabilities of the combining channel W_N in Eq. (2) can be rewritten as

$$W_N(Y_1^N, H_1^N|u_1^N) = \prod_{a \in S_D} W(Y_a, H_a|X_a). \tag{15}$$

and the polarized bit-subchannels are redefined as

$$W_N^{(i)}\left(Y_1^N, H_1^N, u_1^{i-1}|u_i\right) = \sum_{u_{i+1}^N \in \mathcal{X}^{N-i}} \frac{1}{2^{N-1}} W_N\left(Y_1^N, H_1^N|u_1^N\right). \tag{16}$$

Similar to the single-channel case, it is proved that with$N \to \infty$, some of the polarized subchannels tend to be completely noised, and the others tend to be noise-free, where the fraction of the latter approaches the average symmetric capacity of the underlying component channels [39]. For finite-length polar coding over OFDM parallel channels in this paper, the problem of simple and accurate estimation of polarized subchannel error probability is still largely unsolved. Possible approaches include tracking lower and upper bounds on Bhattacharyya parameters $M\left(W_N^{(i)}\right)$ [14] of the bit subchannels $W_N^{(i)}$, as shown in Eq. (14). However, these bounds are not guaranteed to be tight.

$$M\left(W_N^{(i)}\right) = \sum_{Y_1^N \in \mathcal{Y}^N, H_1^N \in \mathcal{H}^N} \sum_{u_1^{i-1} \in \mathcal{X}^{i-1}} \sqrt{W_N^{(i)}\left(Y_1^N, H_1^N, u_1^{i-1}|0\right) W_N^{(i)}\left(Y_1^N, H_1^N, u_1^{i-1}|1\right)}. \tag{17}$$

Monte-Carlo simulations were suggested in [31, 34] in order to find good subchannels in the case of the Rayleigh fading channel with known channel distribution. However, neither of these works provide simple techniques to evaluate the bit error probability of the subchannels induced by the polarizing transformation. To reduce $M\left(W_N^{(i)}\right)$ parameters' excessive computational complexity, in the next section, we propose a novel polar code construction method for the above proposed UWA OFDM polarized bit-subchannels with known CSI.

3.2 Polar code construction for the UWA channel

In this section, we propose a novel polar code construction method based on the MC simulation method and the GA method [19] with details of the specific implementation.

Given the proposed slow fading OFDM UWA channel model in the Eq. (14), for a BPSK constellation, when the channel parameter is available at the receiver, the LLR $l(a, n_{bl})$ on the subcarrier $a \in S_D$ of n_{bl} - th OFDM block signal is obtained as

$$l(a, n_{bl}) = \ln \frac{W(Y_a, H_a|1)}{W(Y_a, H_a|-1)} = \frac{2Y_a H_a}{\sigma_a^2} \tag{18}$$

In this case, the $l(a, n_{bl}) \sim \mathcal{N}\left(2H_a^2/\sigma_a^2, 4H_a^2/\sigma_a^2\right)$, provided that the all-zero codeword is transmitted. The LLR is considered as a Gaussian random variable with $\mathrm{Var}[l(a, n_{bl})] = 2\mathrm{E}[l(a, n_{bl})]$. Here, E and Var are respectively the mean and the variance. Thus, we can use the GA method to evaluate the bit error probability of the subchannels.

For the original GA method, $N = 2^n$ bit subchannels can be obtained for a given binary input AWGN channel (BIAWGNC) $W : \mathcal{X} \to \mathcal{Y}$ by channel polarization. Since the underlying channels for channel polarization are used of the same channel $W : \mathcal{X} \to \mathcal{Y}$, the $L_\lambda(\phi, \beta)$ for each node of the polar factor graph in Fig. 1b can be abbreviated as $L_\lambda(\phi, \beta) = L_\lambda(\phi)$. The $L_\lambda(\phi)$ can be approximated with a set of Gaussian distributions, in which the variance of the distribution is two times the average value. This enables one to compute only the mean value of $L_\lambda(\phi)$, i.e., $\mathbf{E}[L_\lambda(\phi)]$, which drastically reduces the complexity. The mean of the LLRs $\mathbf{E}[L_\lambda(\phi)]$ can be calculated recursively according to the channel polarization process as

$$\mathbf{E}\left[L_N(2i-1)\right] = f^{-1}\left(1 - \left(1 - f\left(\mathbf{E}\left[L_{N/2}(i)\right]\right)\right)^2\right) \tag{19}$$

$$\mathbf{E}\left[L_N(2i)\right] = 2\mathbf{E}\left[L_{N/2}(i)\right] \tag{20}$$

$$\mathbf{E}\left[L_1(1)\right] = 2/\sigma^2 \tag{21}$$

where

$$f(x) \triangleq \begin{cases} \exp\left(-0.4527x^{0.86} + 0.0218\right) & \text{if } 0 < x \le 10 \\ \sqrt{\frac{\pi}{2}}\left(1 - \frac{10}{7x}\right)\exp(-x/4), & \text{if } x > 10 \end{cases} \tag{22}$$

Then the bit error probability for $W_N^{(i)}$ can be evaluated by

$$P_e\left(W_N^{(i)}\right) \approx Q\left(\sqrt{\mathbf{E}\left[L_N^{(i)}\right]/2}\right), 1 \le i \le N \tag{23}$$

where

$$Q(x) = \int_x^{+\infty} \frac{1}{\sqrt{2\pi}} e^{-t^2/2} dt \tag{24}$$

In the OFDM UWC system, since the underlying channels $W:\{W_a|H_a:\mathcal{X}\rightarrow\mathcal{Y}\},a\in S_D$ of the channel polarization transformation are no longer used of the same channel, there is a need to optimize the recursive formula in the GA method for the parallel OFDM channel. As a result, Eqs. (19) and (20) need to be refined as

$$\mathbf{E}\left[L_N(2i-1,m)\right]=f^{-1}\left(1-\left(1-f\left(\mathbf{E}\left[L_{N/2}(i,2m-1)\right]\right)\right)\left(1-f\left(\mathbf{E}\left[L_{N/2}(i,2m)\right]\right)\right)\right) \tag{25}$$

$$\mathbf{E}\left[L_N(2i,m)\right]=\mathbf{E}\left[L_{N/2}(i,2m-1)\right]+\mathbf{E}\left[L_{N/2}(i,2m)\right] \tag{26}$$

Next, further refinement of the polar code construction steps based on the GA method proposed above. Considering the uncertainty of UWA channels cannot be characterized and fading statistics are not available, we use the MC simulation-based method to find the information set. To construct polar codes in the proposed dynamic slow time-varying UWC channel, a set of random realizations of $H(f,t)$ is generated. Then, for each realization of the fading, the average LLR for a BPSK constellation in each OFDM subcarrier channel is estimated. And the conditional BER of polarized bit-subchannels, v_b^i, is determined using the GA method. After running this for several fading matrix realizations, we take the average over v_b^i through Monte-Carlo statics, and the information set is determined as the K subchannels with the lowest conditional BERs. This method is described in Algorithm 1.

For ease of representation, the mean of LLR $\mathbf{E}[L_\lambda(\phi,\beta)]$ for each node in the recursive Eqs. (25) and (26) are represented as $\bar{l}_\lambda(\phi,\beta)$ according to the factor graph in Fig. 1.

Algorithm 1. MC GA-based Polar Code construction for the OFDM UWA channel

Input: The number of OFDM Block in transmission N_{bl}. The estimated channel transfer function $H(f_a,n_{bl})$. The noise variance $\sigma^2(f_a,n_{bl})$; The code length N;

Output: The sorted bit-channel indices **idx**

for $n_{bl}=1:N_{bl}$ **do**
  for $a=1:N$ **do**
    $\bar{l}_0(0,a-1)=2H^2(f_a,n_{bl})/\sigma^2(f_a,n_{bl})$
  end
  for $j=0:\log_2 N-1$ **do**
    for $i=0:2^j-1$ **do**
      for $m=0:2^{(\log_2 N-j-1)}-1$
        $\bar{l}_{j+1}(2i,m)=f^{-1}\left(1-\left(1-f\left(\bar{l}_j(i,2m)\right)\right)\left(1-f\left(\bar{l}_j(i,2m+1)\right)\right)\right)$ (27)
        $\bar{l}_{j+1}(2i+1,m)=\bar{l}_j(i,2m)+\bar{l}_j(i,2m+1)$ (28)
      end
    end
  end
  for $\kappa=1:N$ **do**
    $v_{\kappa,n_{bl}}=Q\left(\sqrt{\bar{l}_{\log_2(N)}(\kappa,0)/2}\right)$
  end
end
$\mathbf{v}_\kappa=\sum_{n_{bl}}\mathbf{v}_{\kappa,n_{bl}}/N_{bl}$
$[\mathbf{idx}]=sort\left([\mathbf{v}_1,\mathbf{v}_2,\ldots,\mathbf{v}_N]\right)$
Return **idx**

The complexity of the proposed method can be estimated as $\mathcal{O}(N_{bl}N)$, which is much less than the complexity $\mathcal{O}(N_{bl}N\log N)$ of the original MC simulation method [14, 31]. The concrete steps for the proposed polar code construction in OFDM UWC systems are given as follows.

(1) At the transmitter end, set the given all-zero vector of length N as the sample binary sequence u_1^N, of which all bits are treated as frozen bits in the SC decoder. Then generate the polar codeword x_1^N by the encoding operation. Afterward, following the BPSK mapping, create an OFDM block by OFDM modulation. Repeat the above process to generate N_{bl} OFDM blocks as Monte-Carlo sample signals for multiple repeated transmissions.

(2) At the receiver end, firstly, accurate channel estimation is very helpful to quantify the reliability of the polarized bit-subchannels more accurately. Since the transmit sequence in step (1) is known on both the transmitting and receiving sides, we can use it as a reference sequence to perform the least-squares (LS) channel estimation. Through accurate channel estimation and noise measurements, we can determine the real-time channel state information (CSI) of $\hat{H}_a(n_{bl})$ and noise variance $\sigma_a^2(n_{bl})$. Then enter these two parameters of the UWA channel into Algorithm 1 to initialize $\bar{l}_0(0,a), a \in S_D$,i.e., the mean of LLR distribution $L_0(0,i)$ and calculate the BER of all polarized subchannels.

(3) According to the output result of Algorithm 1 and the code rate $R \triangleq K/N$, select K good bit-channels $\mathcal{A}$ out of N to transmit information bits while distributing frozen bits to other $N-K$ bit-channels $\mathcal{A}^c$ As of now, the polar code construction for the UWC is completed.

Detailed information on the system parameters and application processes for this method can be found in the following section.

4 Polar coded OFDM UWC system model

To verify the polar code construction method proposed in Section III and analyze the application performance of polar code in the UWC OFDM system, in this section, we establish a practical and reliable polar coded UWC scheme by devising a two-step procedure.

The first step is polar code construction, which is considered as the channel prediction /data preprocessing for the second step. A detailed description of this step is given in Section III-B. The application processes at the transmitter and receiver are shown in the dashed boxes in Fig. 3a, b, respectively. At the end of the step, the result of polar code construction is fed back to the transmitter as a signaling message through a feedback link and assumed that the feedback delay has little effect on the performance.

The second step is the adaptive coding UWC, which is to encode the original input sequence based on the results of the polar code construction from step one and then implement OFDM UWC. The UWC processes at the transmitter and receiver are shown in the solid boxes in Fig. 3a, b, respectively.

Next, the function modules and parameter settings in the system model are introduced in detail.

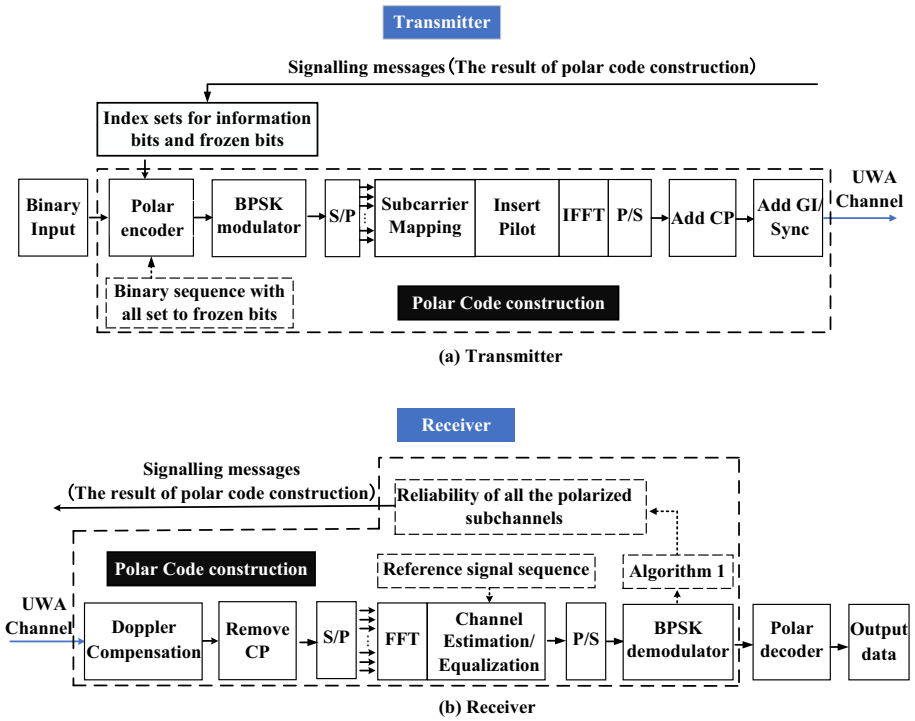

Fig. 3 Schematic diagram of the polar-coded OFDM UWC system

In Fig. 3a, at the transmitter, the binary input signal $U : \{u_i, 1 \le i \le K\}$ is first encoded with a polar code $X : \{x_j, 1 \le j \le N\}$ at the code rate $R \triangleq K/N$. With Binary Phase Shift Keying (BPSK) modulation, the output of the polar encoder is mapped into $S : \{s_i = (1 - 2x_i)\sqrt{E_b}\}, x_i \in \{0, 1\}$, where $E_b = 1$ is bit energy. Then data stream is processed by OFDM. Considering cyclic-prefixed (CP) OFDM block transmission, let T denote the basic OFDM symbol duration, which dictates a subcarrier spacing Δf of $1/T$. Assume A subcarriers in total. The a-th subcarrier is located at the frequency $f_a = f_c + a/T$, $a = -A/2, \ldots, A/2 - 1$, where $f_c = 12000$ Hz is the center frequency. Serial data streams V are converted into parallel streams and allocated to subcarriers, into which the comb-type pilot is also inserted at subcarrier intervals of $\Delta S_p = 4$. After inverse fast Fourier transform (IFFT), the CP of duration T_{cp} is inserted in front of the OFDM symbol as a guard interval (GI) to avoid ISI. Let $s_a(n_{bl})$ denote the symbol on the a-th subcarrier of the n_{bl}-th block. Then the passband signal of the n_{bl}-th transmitted block can be expressed as

$$s(t; n_{bl}) = 2\mathrm{Re}\left[\left(\sum_{a \in S_A} s_a(n_{bl}) e^{j2\pi \frac{a}{T} t} g(t)\right) e^{j2\pi f_c t}\right], t \in \left[-T_{\mathrm{cp}}, T\right], \tag{29}$$

where S_A denotes the set of active subcarriers and $g(t)$ is a rectangular window of length $T + T_{cp}$ defined as

$$g(t) = \begin{cases} 1/T & t \in \left[-T_{\mathrm{cp}}, T\right] \\ 0 & \text{otherwise} \end{cases}. \tag{30}$$

Table 1 Parameters of the polar-coded OFDM System

Parameters	Description	Value
f_c	Carrier frequency	12 kHz
B	Bandwidth	8 kHz
f_s	Sampling frequency	48 kHz
A	Number of subcarriers	341
Δf	Subcarrier bandwidth	23.4375 Hz
ΔS_p	Pilot Spacing	4
T	Symbol duration	42.7 ms
T_{cp}	Cyclic prefix	10.7 ms
T_g	Guard interval	300 ms
N_{bl}	Blocks in each transmission	20
N	Polar code length	256
R	Polar code rate	1/2,3/4
R_D	Data rate	3.2 kb/s, 4.8 kb/s

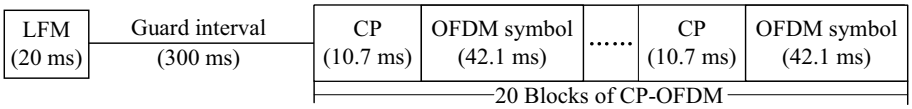

Fig. 4 The frame structure of the transmitted signal

For each transmission with $N_{bl} = 20$ OFDM blocks configured with the parameters shown in Table 1, the transmitted signal is

$$s(t) = \sum_{n_{bl}=1}^{N_{\mathrm{bl}}} s\big(t - n_{bl}(T_{\mathrm{cp}} + T)\big), \quad t \in \big[0, N_{\mathrm{bl}}(T_{\mathrm{cp}} + T)\big]. \tag{31}$$

For synchronization, a linear frequency-modulated (LFM) waveform with a time duration of $T_g = 20$ ms and a bandwidth of 4 kHz was inserted before them. The structure of the transmitted signal is presented in Fig. 4.

In Fig. 3b, at the receiver, assuming that $T_{\mathrm{cp}} > \tau_{\max}$. When $t \in [n_{bl}(T_{\mathrm{cp}} + T), n_{bl}(T_{\mathrm{cp}} + T) + T]$ and $\tau \in [0, \tau_{\max}]$, we have $g(t - \tau) = 1/T$. A closed-form expression of the received signal within the interval $t \in [n_{bl}(T_{\mathrm{cp}} + T), n_{bl}(T_{\mathrm{cp}} + T) + T]$ is

$$\begin{aligned} \tilde{y}(t; n_{bl}) &= \int_0^{\tau_{\max}} h(\tau, t) 2\mathrm{Re}\left\{ \frac{1}{T} \sum_{a \in S_{\mathrm{A}}} s_a(n_{bl}) e^{j2\pi f_a (t-\tau)} \right\} d\tau \\ &+ \tilde{z}(t; n_{bl}) = 2\mathrm{Re}\left\{ \frac{1}{T} \sum_{a \in S_{\mathrm{A}}} H_a(n_{bl}) s_a(n_{bl}) e^{j2\pi f_a t} \right\} + \tilde{z}(t; n_{bl}), \end{aligned} \tag{32}$$

where $H_a(n_{bl})$ is the channel transfer function at the a-th subcarrier of the n_{bl}-th OFDM block. Moreover, $\tilde{z}(t; n_{bl})$ denotes ambient noise and site-specific noise on the n_{bl}-th OFDM block, following $\tilde{z}(t; n_{bl}) \sim \mathcal{CN}\big(0, \sigma_a^2\big)$ [9]. After doppler compensation and

removing CP, performing the Fourier transform on the truncated waveform of duration T, we have

$$\tilde{Y}(f;n_{bl}) = \int_0^T \tilde{y}(t;n_{bl})e^{-j2\pi ft}dt = \sum_{a\in S_A} H_a(n_{bl})S_a(n_{bl})G_{\text{rec}}(f-f_a)+\tilde{Z}(f,n_{bl}), \quad f>0, \tag{33}$$

Draw the samples on the subcarrier frequencies f_a. We have

$$Y_a(n_{bl}) = H_a(n_{bl})S_a(n_{bl}) + Z(f,n_{bl}), \tag{34}$$

where

$$H_a(n_{bl}) = H_d(f,n_{bl})|_{f=f_a} = Q(d,f_a)B(f_a,n_{bl}). \tag{35}$$

Channel estimation for the OFDM system can be performed in the frequency domain. In the first step of the proposed UWC scheme, the channel estimation flow is as described in Section III-B. And in the second step, the estimated CSI of $\hat{H}_a(n_{bl})$ is estimated based on pilot tones via the LS estimator and interpolation scheme. For simplicity, we assumed perfect channel estimation, and therefore $\hat{H}_a(n_{bl}) = H_a(n_{bl})$, the observation $\hat{S}_a(n_{bl})$ obtained by

$$\hat{S}_a(n_{bl}) = \frac{Y_a(n_{bl})}{\hat{H}_a(n_{bl})} = S_a(n_{bl}) + \frac{Z(f,n_{bl})}{H_a(n_{bl})}, \tag{36}$$

The noise variance σ_{na}^2 is obtained by the noise power when there is no signal transmission. After BPSK demodulation, we initialize the polar decoder with soft metrics, in the form of the LLR vector $l(a,n_{bl})$ as shown in Eq. (18). Then, the estimated message vector $\hat{u}_i$ can be obtained by the SC, SCL, BP, and SCAN decoding methods as described in Section II-B.

5 Simulation results

Simulations are performed in this section to verify and evaluate the performance of the proposed polar construction method in Section III and the polar coded OFDM UWC scheme in Section IV.

5.1 Simulation setup

The parameters of the polar coded OFDM UWC system are specified in Table 1. Th slow time-varying UWA channel in simulations is described with WSSUS assumption for the statistical part, and its CIR $h(\tau,t)$ is

$$h(\tau,t) = \sum_{p=1}^{P} A_p e^{j2\pi\nu_p t}\delta(\tau-\tau_p), \tag{37}$$

where P is the number of arrival paths. And A_p, τ_p and ν_p denote the cumulative reflection coefficient, the time delay, and the Doppler shift along the p-th propagation path, respectively.

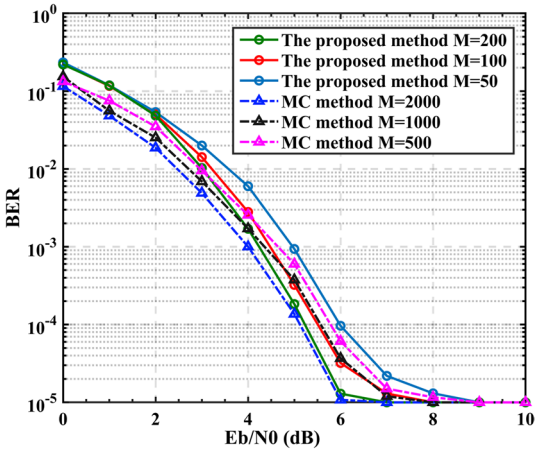

Fig. 5 BER Performance of the proposed polar code construction method and original Monte-Carlo (MC) method in the UWC system. $N = 256$, $R = 0.5$

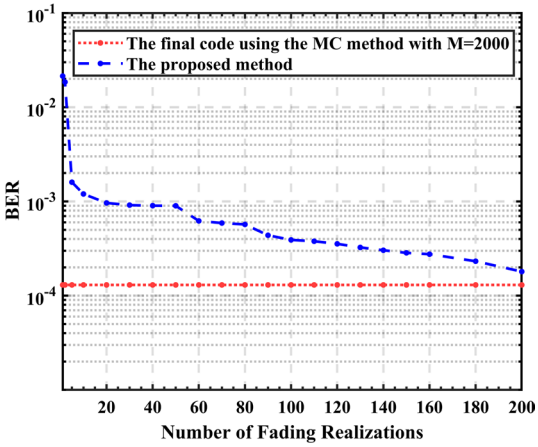

Fig. 6 Evaluation of the effect of the number of fading realizations on the BER for the proposed polar code construction method. SNR = 6 dB, $N = 256$, $R = 0.5$

In the simulation, set $A = [1,0.42,0.28,0.14,0.07, 0.02]$ [37]. Assume the random doppler shifts v_p are distributed according to a Jakes Doppler spectral density as given by [40–42]

$$p_v(v) = \frac{1}{\pi f_{\max}\sqrt{1-\left(v/f_{\max}\right)^2}},\ |v| < f_{\max}, \tag{38}$$

where $f_{\max}$ denotes maximum Doppler shift and is set to $f_{\max} = 10^{-2}\Delta f$, where Δf is subcarrier bandwidth. Assume that the delays τ_p are distributed Delay power spectrum as given by

$$p_\tau(\tau) = \frac{1}{\tau_{rms}(1-e^{-\frac{|\tau|}{\tau_{\max}}})}e^{-\frac{|\tau|}{\tau_{\max}}},\ 0 \le \tau \le \tau_{\max}, \tag{39}$$

where $\tau_{\max}$ denotes maximum multiway delay and τ_{rms} denotes the root mean square of $\tau_{\max}$. Set $\tau_{\max} \leq T_{cp}$, where T_{cp} is CP duration. In the following simulations, the UWA channel will be simulated according to the above specification.

5.2 BER performance of the proposed polar code construction algorithm for the UWA channel

In this section, the BER performance of the proposed MC GA-based construction method for the UWC system is presented in Fig. 4. Moreover, to demonstrate the superiority of the proposed method, the BER curve of the original MC simulation construction method [14, 31] is also plotted.

For each signal-to-noise ratio (SNR), in the polar construction process, fix the polar code length N to be 256. Vary the Monte-Carlo iteration number M, i.e., the number of OFDM blocks in transmission N_{bl}, from 1 to 2000. The adaptive coding UWC processes are simulated 1,000 times to measure the average BER of the UWC system. In this process, the code rate R is fixed to be 0.5, and the SC decoder is used as the polar decoder. The results for various numbers of Monte Carlo iterations and SNRs are shown in Figs. 5 and 6.

Figure 5 shows that the original Monte-Carlo simulation method can achieve BER between 10^{-4} and 10^{-5} at an SNR of 6 dB with 50, 1000, and 2000 times iteration, ensuring reliable communication in the UWA channel. As M decreases from 2000 to 500, the BER performance is reduced by 0.4–0.8 dB. The proposed construction method significantly reduces the number of iterations to 50, 100, and 200, while still achieving comparable performance to the original MC simulation method. For signal-to-noise ratios in the range of 7–10 dB, the construction method proposed in this paper achieves comparable performance to the original MC simulation method for error-free transmission, while significantly reducing the number of iterations. The results are consistent with those for signal-to-noise ratios of 0–6 dB. Moreover, Fig. 6 shows the number of Monte-Carlo iterations, i.e., the fading realizations, needed in the proposed method to achieve the lowest BER at the SNR of 5 dB using the original MC method with $M = 2000$. It can

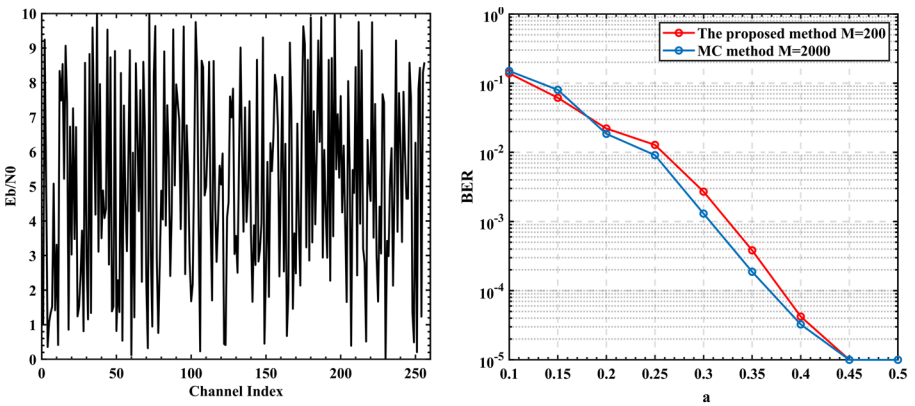

(a) Signal to noise ratio for each Gaussian parallel channel (b) BER performance of the two algorithms as a varies

Fig. 7 BER Performance of the proposed polar code construction method and original Monte-Carlo (MC) method in the AWGN channel. $N = 256$, $R = 0.5$

be seen that with only 100 to 200 times iterations, we can design the best code found using the original MC simulation approach. The complexity of the proposed method can be estimated as $\mathcal{O}(MN)$, which is much less than the complexity $\mathcal{O}(MN \log N)$ of the original MC simulation method. Therefore, the proposed method is more suitable for the polar code construction in UWA channels with short coherence time and meets the need for reliable communication.

Moreover, the BER performance of the proposed MC GA-based construction method for the AWGN channel is presented in Fig. 7. Since the method proposed in this paper extends to parallel, heterogeneous, slow time-varying Gaussian channels, to simulate the performance of the proposed construction method and the original Monte Carlo method in a Gaussian channel, we set up a set of 256 mutually independent parallel Gaussian channels with different variances of additive Gaussian noise $\sigma_i^2, i = 1 \ldots 256$ on each channel. The $(E_b/N_0)_i, i = 1 \ldots 256$ value of each channel can be assumed to be the value in the Fig. 7a, and a uniformly distributed random number is added to this value to simulate the variation characteristics of each Gaussian channel. In order to obtain the simulation performance results under multiple SNRs, a multiplicative factor a is set, and the performance of the two algorithms in each Gaussian parallel channel under $a \cdot (E_b/N_0)_i, i = 1 \ldots 256$ is simulated, and the results are shown in Fig. 7b.

Based on the results in Fig. 5, for each SNR level, the number of Monte-Carlo iterations during the proposed polar construction process is fixed to be 200, and running 1000 communication simulations and measuring the average BER. During the simulations, set it to BER = 1e−5 when BER equals 0. As can be seen from the results in Fig. 7, as a increases, the signal-to-noise ratio of each channel increases and the BER of the two algorithms under AWGN channels gradually decreases to BER-free. The construction method proposed in this paper achieves comparable performance to the original MC simulation method while greatly reducing the number of iterations, and this result is consistent with that in UWA channels.

To further explore the performance variation of channel estimation optimization during the polar code construction process, the BER of BPSK demodulation before and after optimization of channel estimation is given in Fig. 8a. The results in the figure show that

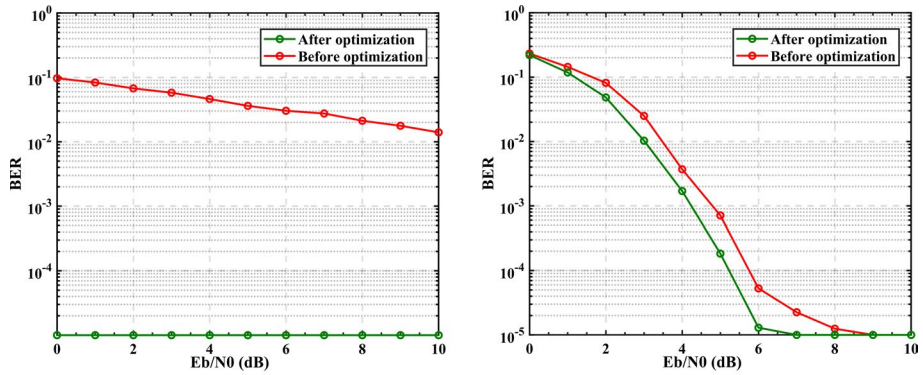

(a) The BER of BPSK demodulation before and after channel estimation optimization.

(b) BER of the adaptive coded communication using the polar code

Fig. 8 BER performance variation of channel estimation optimization during the polar code construction process. $N = 256$, $R = 0.5$

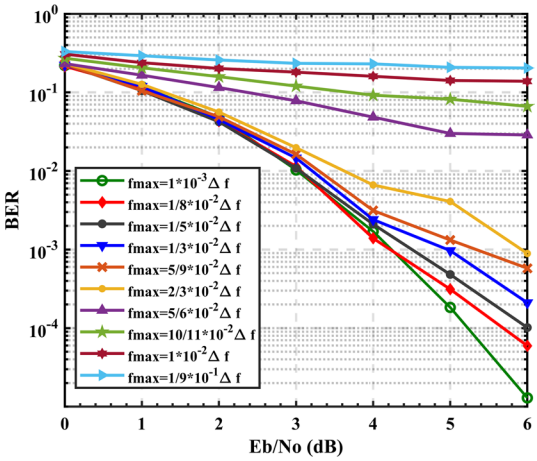

Fig. 9 Variation of BER with channel Doppler for Polar coded-OFDM UWC system. $N = 256$, $R = 0.5$

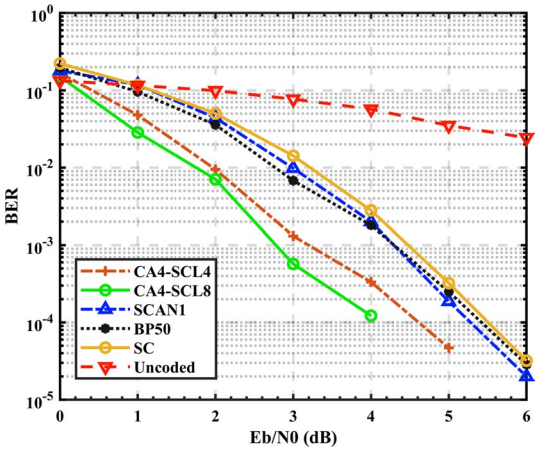

Fig. 10 BER Performance comparison of four polar decoders in the UWC system. $N = 256$, $R = 0.5$

the optimized channel estimation method uses the transmitted signal as the reference sequence, which can achieve BER-free BPSK demodulation and provide more accurate channel parameters for polar code construction. Based on this, the BER of adaptive coded communication using the polar code construction results before and after the optimized channel estimation is presented in Fig. 8b. The results in the figure show that there is a performance gain of approximately 0.4–0.8 dB after the optimized channel estimation, compared to that before the optimization.

5.3 Robustness to slow time-varying channels

Channels are time-varying during polar code construction and adaptive coding communication. To provide reference values for the subsequent fault tolerance of Doppler estimation and compensation, this section analyzes the robustness of the system to the time-varying channel caused by Doppler. Assuming that Doppler exists and does not compensate for it, the bit error rate of the system under each SNR is observed. During the simulation process, fix the polar code length to be 256 and the code rate to be 0.5.

For each SNR level, the number of Monte-Carlo iterations during the proposed polar construction process is fixed to be 200, and running 1000 communication simulations and measuring the average BER. Change the maximum Doppler frequency shift $f_{\max}$ from $1 \times 10^{-3} \triangle f$ to $1/9 \times 10^{-1} \triangle f$, where is the sub-carrier bandwidth $\triangle f$, and the channel Doppler distribution is as in Eq. (30). The multipath and maximum delay remain unchanged, and the results are shown in Fig. 9.

With increasing Doppler frequency shifts, the simulation results indicate that the system BER increases without Doppler compensation. When $f_{\max} \leq 2/3 \times 10^{-2} \triangle f$, the system bit error rate can reach about 10^{-3} within 6 dB, realizing reliable communication. When $f_{\max} \geq 5/6 \times 10^{-2} \triangle f$, the BER can only reach 10^{-1}, and the polar code cannot be effective in error correction.

5.4 BER performance comparison of the polar decoders

In this section, based on the proposed polar code construction method in this paper, the performance of the polar coded OFDM UWC scheme is studied. Figure 10 shows the BER performance comparisons of the scheme under the SC, CRC-aided SCL(CASCL), BP, and SCAN decoders. In this simulation, fix the polar code length to be 256 and the code rate to be 0.5. For each SNR level, the number of Monte-Carlo iterations during the proposed polar construction process is fixed to be 200, and running 1000 communication simulations and measuring the average BER.

The OFDM UWC system under four polar decoders can all achieve BER at the magnitude of 10^{-4} within 5 dB, ensuring reliable communication in the UWA channel. The system performance under the SC decoder, SCAN decoder with one iteration, and BP decoder with 50 iterations are similar. It can be seen that the SCAN decoder has faster convergence and achieves similar performance to the SC decoder with only one iteration, whereas the BP decoder needs at least 50 iterations. Moreover, the CRC-aided SCL decoder with list size $L = 4$ and a 4-bit CRC outperforms the previous three decoders with around a 0.5–1.1 dB gap. It can be found that increasing list size from 4 to 8 improves BER only slightly. Therefore, a CASCL decoder with list size $L = 4$ and a 4-bit CRC will be used in subsequent simulations and experiments. Moreover, the uncoded

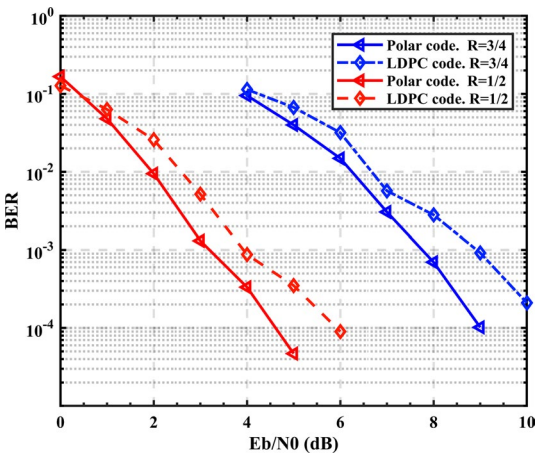

Fig. 11 BER performance of polar-coded, LDPC-coded OFDM UWC system. N = 256

BER curves are also plotted. It shows that the coding performance is greatly enhanced when the uncoded BER is below 0.1. We will further verify the results by the lake trial experiment in section VI. As for decoder parameter settings, we primarily consider the CASCL decoder with a list size of 4 and a 4-bit CRC, the BP decoder with 50 iterations, and the SCAN decoder with one iteration.

5.5 BER performance comparison between polar code and LDPC code

To get insights into the performance comparison between the polar code with the LDPC code, we fix the code length N to be 256 and the code rate R to be 0.5 and 0.75. Encoding LDPC according to 3GPP TS 38.212 [16, 28]. And the BP decoder with a maximum of 50 iterations is used for LDPC decoding. The number of Monte-Carlo iterations during the proposed polar construction process is fixed to be 200. The CASCL decoding with list size $L = 4$ and a 4-bit CRC is used for the polar decoder. For each SNR level, running 1000 communication simulations and measuring the average BER. The result is shown in Fig. 11.

It depicts that the polar coded UWC scheme under the CRC-aided SCL decoder outperforms the LDPC coded system with around 1.2–2 dB gain. A smaller code rate results in better performance for LDPC codes and polar codes. As shown in Fig. 8, the BER performance of polar code improves by around 4 dB with the code rate increasing from 1/2 to 3/4.

6 Experimental results

6.1 The lake trial experiment setup

To further verify and evaluate the performance of the proposed polar construction method and the proposed polar coded OFDM UWC scheme in the practical application, we conducted the UWC experiment at Qiandao Lake (Xin'an Jiang reservoir), Hangzhou, China, in December 2021. During the experiment, the transmitting transducer was suspended from the dock, while the receiver was suspended from the surface vessel. For communication tests, the surface vessel with receiving transducers was positioned at two locations, namely S1(29°33′5″ N118°57′16″ E), and S2(29°33′20″ N 118°57′49″ E), which are 749 m and 1718 m away from the transmitter (29°33′38″ N118°58′08″ E), respectively. The experiment setup is shown in Fig. 12. The transmitter and the receiver were deployed in the water at a depth of about 10–15 m, where the water temperature is

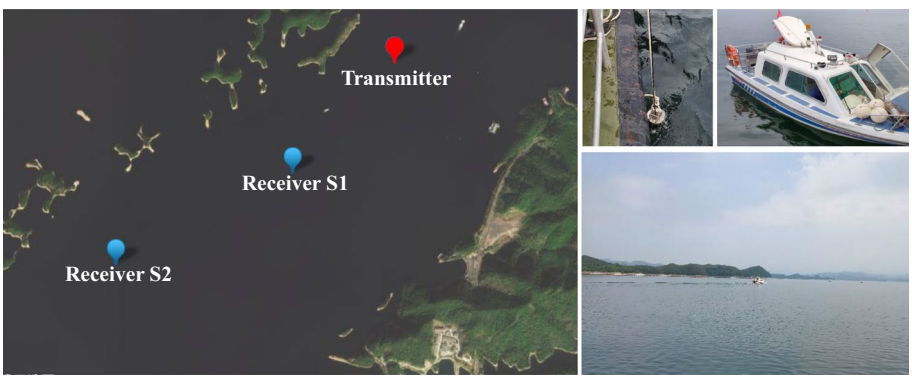

Fig. 12 The lake trial experiment setup

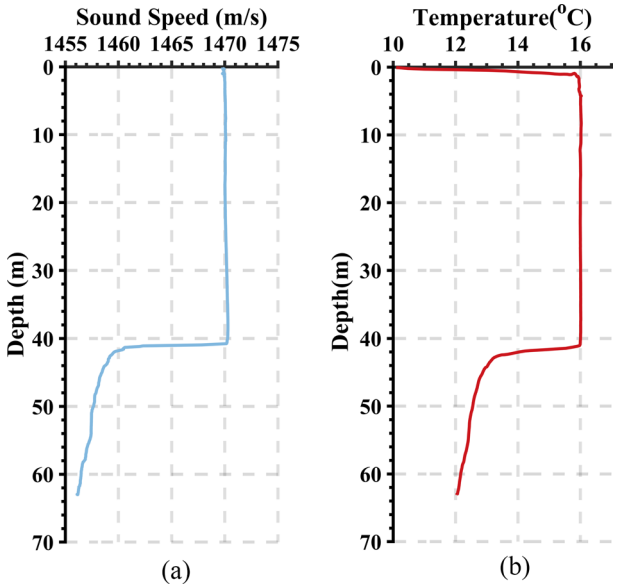

Fig. 13 Experimental environmental measurements. **a** Sound speed profiles. **b** Water temperature

Table 2 Parameter of OFDM UWC system under different polar code lengths *N*

N	**128**	**256**	**512**	**1024**
Δf (*Hz*)	46.88	23.44	11.72	5.86
A	1024	2048	4096	8192
$R_D(kb/s)$	1.6	3.2	6.4	12.8
$T_{cp}(ms)$	5.34	10.67	21.34	42.67
T (*ms*)	21.34	42.67	85.3	170.7

about 16 °C and the sound speed is about 1470 m/s, as shown in Fig. 13. The center frequency of the transducer is 12 kHz with a bandwidth of 8 kHz. The transmitting sound source level is 175 dB re. 1 μPa. The receiving sensitivity is − 185 dB re. 1 V/μPa and the sampling rate is 128 kHz.

Moreover, there are 20 OFDM blocks for each transmission with the parameters specified in Table 1. The bandwidth of the transmission signal is 8 kHz, with a center frequency of 12 kHz. As shown in Table 2, with a polar code length N of 128, 256, 512, and 1024, the duration of one OFDM block is 26.67 ms, 53.35 ms, 106.7 ms, and 213.4 ms. And the duration of each transmission is 533.4 ms, 1067 ms, 2134 ms, and 4268 ms respectively.

In the first step of the proposed OFDM UWC scheme, i.e., the polar code construction, set the binary input sequence as an all-zero vector of length N, with a rate of 0. According to the actual time-varying situation of the channel, N_{bl} transmissions are performed within the time-coherent period to collect Monte-Carlo sample signals. In the second step of the proposed OFDM UWC scheme, i.e., adaptive coding UWC, five transmissions signal containing 100 OFDM blocks are collected for the average BER calculation. As shown in Table 2, when the code rate is set to 1/2, the transmission rate

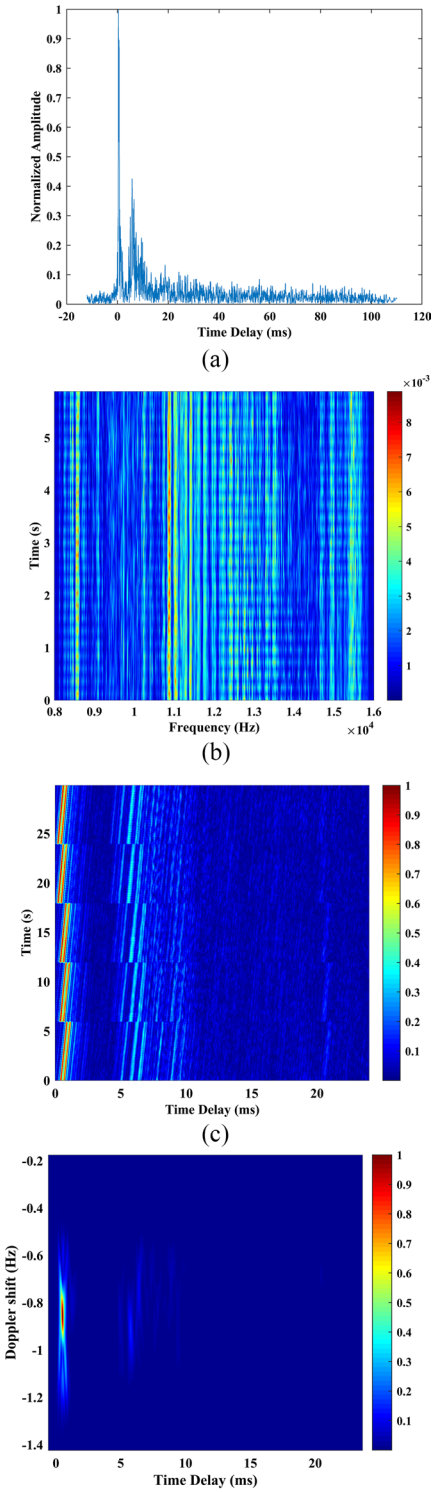

Fig. 14 The channel characteristics at S1. **a** Channel impulse response. **b** The frequency response. **c** Changes over time for the UWA channel. **d** Channel scattering function

with a polar code lengths N of 128, 256, 512, and 1024 are 1.6 kb/s, 3.2 kb/s,6.4 kb/s, and 12.8 kb/s, respectively.

Next, the UWC channel conditions and experiment results at S1 and S2 are given in the following two sections, respectively.

6.2 Experimental results at S1

At first, the channel conditions at the S1 are shown in Fig. 14, including the channel impulse response, the frequency response, the time-varying situation of the channel, and the channel scattering function. Figure 14a shows that there are abundant multipath paths at the S1 point, and the maximum multipath delay is about 10–15 ms. Figure 14b shows that the channel exhibits frequency-selective fading, and the coherence bandwidth is about 67 Hz. Figure 14c indicates that the multipath arrival structure of the channel changes slowly, while the number of multipath components and the delay structure remain constant. The large-scale fading is stable within 25 s. In Fig. 14d, due to the fluctuation of the ship on the sea surface, the maximum Doppler frequency shift in the channel is about 0.85 Hz, and the Doppler spread is approximately 0.2 Hz. Then the coherence time is about 5 s. And the channel variation can be regarded as a slow time variation relative to the duration of the transmitted signal. Therefore, it can support channel prediction and polar code construction results for at least 5 s in advance by appropriate Doppler compensation.

For the polar code construction, in light of the above channel time-varying characteristics and the simulation results of the number of Monte Carlo iterations in Section V-B, we collect five transmissions of signal, which contain 100 OFDM blocks. The duration of the collected signal is about 2.67 s and 5.335 s with the polar code length of 128 and 256 respectively. In Table 3, we present the BER performance of the polar coded OFDM UWC system at a transmission distance of 749 m with a code rate R of 0.5, under SC, CASCL, BP, and SCAN decoders. Moreover, the BER performance of the LDPC coded UWC system is also given. The BP decoder with a maximum of 50 iterations is used for LDPC decoding. The code length is $N = 256$ and the code rate is $R = 0.5$.

As shown in Table 3, the received SNR is around 16.4–17.1 dB, and the uncoded BER is from 0.117 to 0.118. Both channel coding methods in the OFDM UWC system can effectively reduce the error rate in this case. It shows that the polar coded system with code length $N = 128, 256$ and code rate $R = 0.5$ achieve error-free transmission under the SC decoder and CASCL decoder. However, under the BP decoder and

Table 3 BER performance of the proposed polar-coded UWC system and LDPC-coded system at a transmission distance of 749 m

Code	SNR (dB)	*N*	Uncoded BER	BER			
				SC	CA4 SCL4	BP 50	SCAN 1
Polar	17.1	128	0.118	0	0	9.4e−03	4.7e−03
	16.4	256	0.117	0	0	9.0e−3	5.8e−03
LDPC	16.8	256	0.118	3.9e−03			

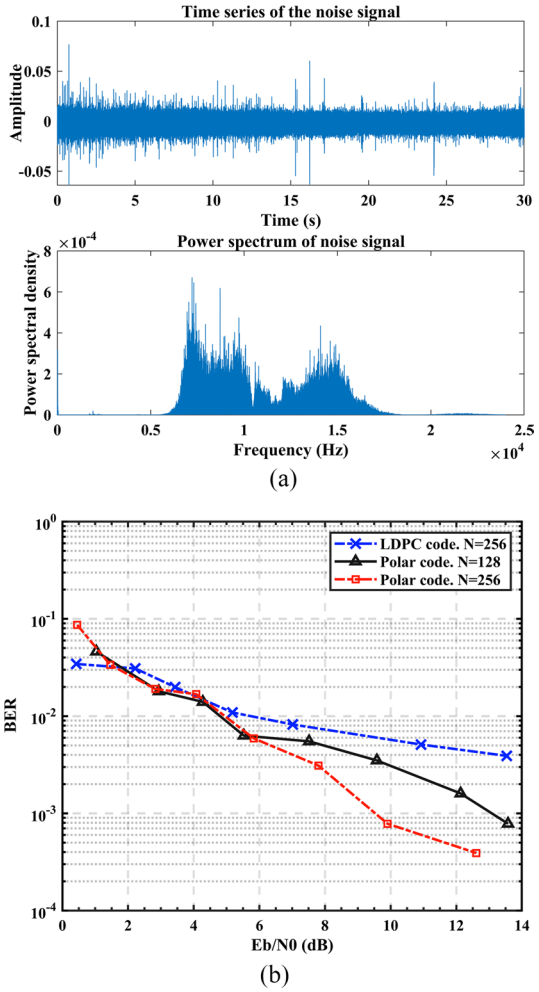

Fig. 15 **a** Ambient noise at S1. **b** Semi-experimental BER versus SNR of the proposed polar-coded UWC system and LDPC-coded system at a transmission distance of 749 m

SCAN decoder, the BER is at the magnitude of 10^{-3}, which is slightly worse than that of the LDPC coded system with code length $N = 256$ and code rate $R = 0.5$.

Furthermore, to test the performance of the proposed polar coded scheme under different SNR levels, inspired by the [9], the ambient noise as shown in Fig. 15a, obtained from the experimental recordings during no signal transmission, is added to the received signal to create a semi-experimental data set. Each SNR dataset includes 100 noise-added OFDM blocks signal for the first step and 100 noise-added OFDM blocks signal for the second step. The BER comparison between the polar coded system under the CASCL decoder and the LDPC coded system is shown in Fig. 15b.

Further statistical tests reveal that the BER performance of the polar coded UWC system is worse than the LDPC coded one when the SNR is in the range of 0–2 dB. With the increase in SNR, LDPC coded system gradually loses the advantage. At the SNR of 10 dB, the proposed polar coded UWC scheme with code length 256 and code rate 0.5 reaches a BER of 10^{-4}, whereas the LDPC coded system only reaches a BER of 10^{-3} in the same case. We can see that polar code outperforms LDPC with an estimated gain

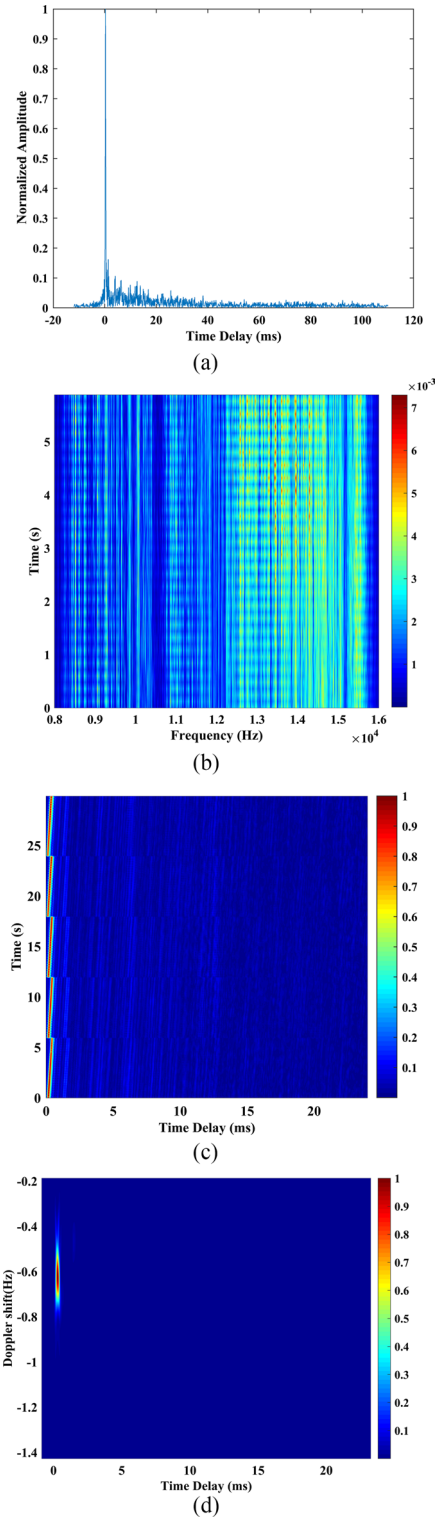

Fig. 16 The channel characteristics at S2. **a** Channel impulse response. **b** The frequency response. **c** Changes over time for the UWA channel. **d** Channel scattering function

of around 1.5–6.4 dB under the CASCL decoder. Furthermore, the polar code length increases from 128 to 256, resulting in a performance gain of about 3.5 dB.

6.3 Experimental results at S2

The channel conditions at S2 are better than those at S1. At S2, the impulse responses are shown in Fig. 16a. It has a simpler multipath structure and less delay span within 5 ms. Figure 16b shows that the channel exhibits frequency-selective fading, and the coherence bandwidth is about 200 Hz. It can be seen from Fig. 16c that the multipath arrival structure and the number of multipath components of the channel are stable within 25 s. In Fig. 16d, due to the fluctuation of the ship on the sea surface, the maximum Doppler frequency shift in the channel is about 0.62 Hz, and the Doppler spread is approximately 0.1 Hz. Then the coherence time is about 10 s. Then the channel variation can be regarded as a slow time variation relative to the transmitted signals. Therefore, it can support channel prediction and polar code construction results for at least 10 s in advance by appropriate Doppler compensation.

For the polar code construction, in light of the above channel time-varying characteristics and the simulation results of the number of Monte Carlo iterations in Section V-B, we collect five transmissions of signal, which contain 100 OFDM blocks. The duration of the collected signal is about 2.67 s, 5.335 s, 10.67 s, and 21.34 s with the polar code length of 128 and 256, 512, and 1024 respectively. In Table 4, we summarize the BER performance of polar coded OFDM UWC system with code lengths $N = 128, 256, 512, 1024$ and code rate $R = 0.5$ under SC, CASCL, BP, and SCAN decoders. Moreover, the BER performance of the LDPC coded system with code length $N = 256$ and code rate $R = 0.5$ is also given.

As can be seen in Table 4, the received SNR is around 20.6–21.9 dB. With code length $N = 128$ and code rate $R = 0.5$, the polar coded system achieves error-free transmission under the CASCL decoder, whereas under the SC, BP, and SCAN decoder, the BER is at the magnitude of 10^{-3}. Meanwhile, with code length $N = 256, 512, 1024$ and code rate $R = 0.5$, there is no error under all the studied polar decoders.

In addition, under the CASCL decoder, the BERs at different polar code rates were also evaluated. The results show that there is no error with the code rate $R = 0.25$ when the received SNR of 20.6 dB, and the uncoded BER is 0.093. The BER with code rate $R = 0.75$ is 0.01375 at the received SNR of 21.3 dB with the uncoded BER 0.086.

Table 4 BER performance of the proposed polar coded UWC system and LDPC coded system at a transmission distance of 1718 m

Code	SNR (dB)	*N*	Uncoded BER	BER			
				SC	CA4 SCL4	BP 50	SCAN1
Polar	20.6	128	0.093	2.3e−03	0	4.7e−03	3.5e−03
	21.4	256	0.087	0	0	0	0
	21.0	512	0.061	0	0	0	0
	21.1	1024	0.056	0	0	0	0
LDPC	21.9	256	0.093	0			

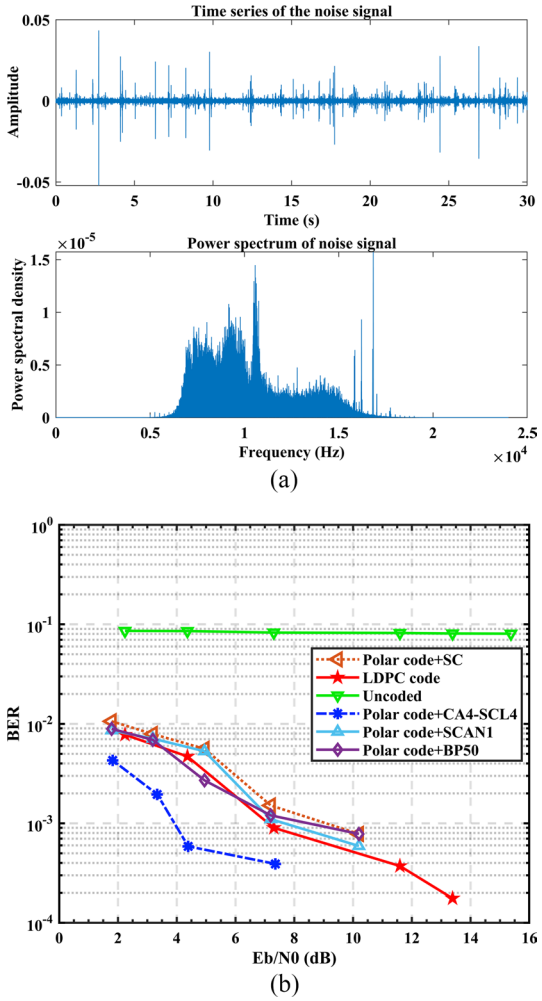

Fig. 17 **a** Ambient noise at S2. **b** Semi-experimental BER versus SNR of the proposed polar-coded UWC system and LDPC-coded system at a transmission distance of 1718 m

Moreover, the LDPC coded system with code length $N = 256$ and code rate $R = 0.5$ achieves error-free transmission at the received SNR of 21.9 dB.

Furthermore, to test the performance of the proposed polar coded scheme under different SNR levels, inspired by the [9], the ambient noise as shown in Fig. 17a, obtained from the experimental recordings during no signal transmission, is added to the received signal to create a semi-experimental data set. Each SNR dataset includes 100 noise-added OFDM blocks signal for the first step and 100 noise-added OFDM blocks signal for the second step. Figure 17b shows the BER performance of the polar coded system under four studied polar decoders. The BER curve of the LDPC coded system with code length $N = 256$ and code rate $R = 0.5$ is also plotted.

As revealed in Fig. 14b, both the proposed polar coded OFDM UWC system and LDPC coded one achieve BERs of the magnitude of 10^{-4} within 10 dB. Among all the studied decoding methods, the SCAN, BP, and SC decoders have similar performance in terms of BER, which is slightly worse than that of the LDPC coded system with an about 2 dB gap. The CASCL decoder outperforms the other three decoding methods

with about a 2.5–5.9 dB gap. It also depicts that the proposed polar coded scheme under the CASCL decoder outperforms the LDPC coded system by approximately 2.1–3.7 dB.

7 Conclusion

In this paper, for the SISO OFDM UWC in the slow time-varying shallow sea channel, a novel polar code construction method was established based on the MC and GA methods. Compared with the original MC simulation method, the proposed method can drastically reduce the complexity from $\mathcal{O}(MN \log N)$ to $\mathcal{O}(MN)$. And the simulation results show that it only takes $M = 100$ to $M = 200$ iterations to achieve the performance of the original MC simulation method with $M = 2000$ iterations. Therefore, the proposed method is more suitable for the polar code construction in UWA channels with short coherence time and meets the need for reliable communication. Next, based on the proposed construction method, we establish a practical polar coded UWC scheme by devising a two-step procedure. After that, simulations and lake trials are conducted to verify its feasibility and analyze its performance. The simulation results demonstrate that the proposed polar coded UWA OFDM system could guarantee reliable data transmission, which achieves BER at the magnitude of 10^{-4} within 6 dB. At the same time, the construction method can maintain robustness in time-varying channels whose maximum Doppler frequency shift is less than $2/3 \times 10^{-2} \triangle f$, where $\triangle f$ is the subcarrier bandwidth. In lake trial experiments, it achieved error-free transmission at a distance of 1718 m with an SNR of 21 dB and a distance of 749 m with an SNR of 16.5 dB. Moreover, under SC decoder, BP decoder with 50 iterations, and SCAN decoder with one iteration, the proposed polar coded UWC system's BER performances are slightly worse than the LDPC coded system. While under CASCL decoder with a list size of 4 and a 4-bit CRC, it outperformed the LDPC coded system, which accord with observations in simulations and semi-experimental.

Abbreviations

AWGN	Additive White Gaussian Noise
BDMC	Binary input discrete memoryless channel
BEC	Binary erasure channel
BP	Belief propagation
CASCL	CRC-aided SCL
CIR	Channel impulse response
CRC	Cyclic redundancy check
CSI	Channel side information
CP	Cyclic-prefixed
DE	Density evolution
DFE	Decision feedback equalization
GA	Gaussian approximation
GI	Guard interval
HARQ	Hybrid automatic repeat request
ISI	Inter-symbol interference
LDPC	Low-density parity-check
LFM	Linear frequency-modulated
LLR	Log-likelihood
MC	Monte Carlo
OFDM	Orthogonal frequency division multiplexing
SC	Successive-cancellation
SCAN	Soft cancellation
SCL	Successive cancellation list
SISO	Single-input-single-output
SNR	Signal-to-noise-ratio
UWA	Underwater acoustic
UWC	Underwater acoustic communication
WSSUS	Wide sense stationary and uncorrelated scattering

Acknowledgements
This work reported herein was funded jointly by Laoshan Laboratory Science and Technology Innovation Project (LSKJ202205105), Key Laboratory Fund (2022-JCJQ-LB-033-07).

Author contributions
YZ carried out experiments, data analysis and drafted the manuscript. JL designed, coordinated and supervised this research. HF participated in the formal analysis of this manuscript. FH participated in the writing-review and editing this manuscript. All authors read and approved the final manuscript.

Availability of data and materials
Not applicable.

Declarations

Competing interest
The authors declare that they have no known competing financial interests or personal relationships that could have appeared to influence the work reported in this paper.

Received: 21 August 2022 Accepted: 24 February 2023
Published online: 09 March 2023

References

1. H. Baalbaki, H. Harb, A.S.K. Rashid et al., LOGO: an efficient local and global data collection mechanism for remote underwater monitoring. J. Wireless. Commun. Network. **2022**, 7 (2022)
2. J. Kim, Cooperative localization for deep-sea exploration using multiple unmanned underwater vehicles. IET Radar, Sonar Navig. **14**(8), 1244–1248 (2020)
3. M. Chitre, S. Shiraz, M. Stojanovic, Underwater acoustic communications and networking: Recent advances and future challenges. Mar. Technol. Soc. J. **42**(1), 103 (2008)
4. Z. Lv, H. Wang, Y. Bai, Research on spatiotemporal fluctuation characteristics of underwater acoustic communication signals. J. Acoust. Soc. Am. **148**(4), 2769–2769 (2020)
5. Y. Labrador et al., Modulation and error correction in the underwater acoustic communication channel. Int. J. Comput. Sci. Netw. **9**(7), 123–130 (2009)
6. L. Huang, Q. Zhang, W. Tan et al., Adaptive modulation and coding in underwater acoustic communications: a machine learning perspective. J. Wireless Commun. Netw. **2020**, 203 (2020)
7. S. Zhou, Z. Wang, *OFDM for Underwater Acoustic Communications* (Wiley, New York, 2014)
8. C. Wang, J. Yin, P. Du et al., Application of orthogonal frequency division multiplexing in cognitive underwater communication. J. Acoust. Soc. Am. **132**(3), 2015–2015 (2012)
9. L. Wan, H. Zhou, X. Xu et al., Adaptive modulation and coding for underwater acoustic OFDM". IEEE. J. Oceanic. Eng. **40**(2), 327–336 (2014)
10. H.W. Jeong, J.W. Jung, I.S. Kim, Non-coherent turbo coded frequency shift keying for reliable covert underwater acoustic communications. J. Acoust. Soc. Am. **151**(4), A235–A235 (2022)
11. J. Xi, S. Yan, L. Xu, Direct-adaptation based bidirectional turbo equalization for underwater acoustic communications: algorithm and undersea experimental results. J. Acoust. Soc. Am. **143**(5), 2715–2728 (2018)
12. S. Liu, Q. Fu, Design optimization of low-density parity check codes in multipath underwater acoustic channels. J. Acoust. Soc. Am. **137**(4), 2214–2214 (2015)
13. E. Ankan, N. Ul Hassan, M. Lentmaier et al., Challenges and some new directions in channel coding. J. Commun. Netw. Kor. **17**(4), 328–338 (2015)
14. E. Arikan, Channel polarization: a method for constructing capacity-achieving codes for symmetric binary-input memoryless channels. IEEE Trans. Inf. Theory **55**(7), 3051–3073 (2009)
15. A. Balatsoukas-Stimming, P. Giard, A. Burg, Comparison of polar decoders with existing low-density parity-check and turbo decoders. In: 2017 IEEE Wireless communications and networking conference workshops (WCNCW). IEEE (2017)
16. 3rd Generation Partnership Project (3GPP) TS 38.212. Multiplexing and channel coding. V.15.1.0 (2018)
17. R. Mori, T. Tanaka, Performance of polar codes with the construction using density evolution. IEEE Commun. Lett. **13**(7), 519–521 (2009)
18. I. Tal, A. Vardy, How to construct polar codes. IEEE Trans. Inf. Theory. **59**(10), 6562–6582 (2013)
19. P. Trifonov, Efficient design and decoding of polar codes. IEEE. Trans. Commun. **60**(11), 3221–3227 (2012)
20. A. Bravo-Santos, Polar codes for the Rayleigh fading channel. IEEE. Commun. Lett. **17**(12), 2352–2355 (2013)
21. K. Niu, Y. Li, Polar codes for fast fading channel: design based on polar spectrum. IEEE Trans. Veh. Technol. **69**(9), 10103–10114 (2020)
22. H. Vangala, V. Emanuele, Y. Hong. A comparative study of polar code constructions for the AWGN channel. arXiv preprint arXiv:1501.02473 (2015)
23. I. Tal, A. Vardy, List decoding of polar codes. IEEE Trans. Inf. Theory. **61**(5), 2213–2226 (2015)
24. E. Arikan, A performance comparison of polar codes and Reed-Muller codes. IEEE Commun. Lett. **12**(6), 447–449 (2008)
25. U.U. Fayyaz, J.R. Barry, Polar codes for partial response channels. In: 2013 IEEE International conference on communications (ICC), Budapest, Hungary. pp. 4337–4341 (2013)

26. P. Giard et al. Hardware decoders for polar codes: an overview. In: 2016 IEEE International symposium on circuits and systems (ISCAS), Montreal, QC, Canada. pp. 149–152 (2016)
27. G. Qiao, S. Xing, F. Zhou, A multi-user detection scheme based on polar code construction in downlink underwater acoustic OFDM communication system. IEEE Access **7**, 65973–65981 (2019)
28. M. Falk, G. Bauch, I. Nissen, On channel codes for short underwater messages. Information **11**(2), 58 (2020)
29. L. Jin, Y. Li, C. Zhao et al., Cascading polar coding and LT coding for radar and sonar networks. J. Wireless. Com. Netw. **2016**, 254 (2016)
30. C. Zhou, C. Hao, L. Qiyun, Joint coding of underwater acoustic communication source channel based on polar code. In: International conference on network communication and information security (ICNCIS 2021). SPIE, 2022.Vol. 12175
31. Y. Zhai, J. Li and H. Feng, Research on Polar coding application for underwater acoustic OFDM communication system. In: 2020 IEEE 6th international conference on computer and communications (ICCC), Chengdu, China. 322–328 (2020)
32. K. Ramesh, R. Vailatha, A novel UC-OFDM framework design based on polar-run-limited encoding (PRLE) scheme and FWFT. Wireless Pers. Commun. **121**(1), 725–744 (2021)
33. O.F. Mahmood, I.B. Jasim, N.H. Qasim, Performance enhancement of underwater channel using polar coded OFDM paradigm. Int. Res. J. Mod. Eng. Technol. Sci. **3**(9), 55–62 (2021)
34. L. Xing, Z. Li, Z. Zhang, et al. Research on the Application of Polar Codes in Underwater Acoustic Communication. In 2021 7th International conference on computer and communications (ICCC). IEEE, 115–119 (2021)
35. V. Lidström, Polar coded non-coherent acoustic underwater communication. In 2021 Fifth underwater communications and networking conference (UComms). IEEE
36. L.I.U. Feng et al., Polar coding aided by adaptive channel equalization for underwater acoustic communication. IEICE. Trans. Fund. Electr. **160**, 83 (2022)
37. C. Polprasert, J.A. Ritcey, M. Stojanovic, Capacity of OFDM systems over fading underwater acoustic channels. IEEE. J. Oceanic. Eng. **36**(4), 514–524 (2011)
38. C.S. Clay, H. Medwin, *Acoustical Oceanography: Principles and Applications* (Wiley, New York, 1977)
39. K. Chen, K. Niu, J.-R. Lin, Practical polar code construction over parallel channels. IET. Commun. **7**(7), 620–627 (2013)
40. P. Amini, R.-R. Chen, B. Farhang-Boroujeny, Filterbank multicarrier communications for underwater acoustic channels. IEEE. J. Oceanic Eng. **40**(1), 115–130 (2014)
41. F.-X. Socheleau, L. Christophe, P. Jean-Michel, Concise derivation of scattering function from channel entropy maximization. IEEE. Trans. Commun. **58**(11), 3098–3103 (2010)
42. S. Kaddouri et al., Least square and trended Doppler estimation in fading channel for high-frequency underwater acoustic communications. IEEE. J. Oceanic. Eng. **39**(1), 179–188 (2013)

Publisher's Note